Microscopic Formation Mechanism of Nanotube Peapods

Savas Berber, Young-Kyun Kwon,* and David Tománek

Department of Physics and Astronomy, Michigan State University, East Lansing, Michigan 48824-1116
(Received 11 January 2002; published 18 April 2002)

Using molecular dynamics calculations, we investigate the absorption of a C_{60} molecule in a $(10, 10)$ nanotube either through the open end or a large defect in the tube wall as possible scenarios for the hierarchical self-assembly of $(C_{60})_n @ (10, 10)$ "nano-peapods." We find the absorption through a defect to be significantly more efficient than the end-on absorption. This process occurs most likely within a narrow launch velocity range for the fullerene that agrees well with the observed optimum temperature window for peapod formation.

PACS numbers: 61.48.+c, 68.70.+w, 81.05.Tp

A new type of self-assembled hybrid structures called "nano-peapods," consisting of fullerene arrays inside single-wall carbon nanotubes, have recently been reported [1–6]. Potential uses of nano-peapods range from nanometer-sized containers for chemical reactions [4] to data storage [7], and possibly high temperature superconductors [8]. Even though the encapsulation of fullerenes (such as C_{60}) in nanotubes is favorable on energetic grounds [7,9,10] and occurs rapidly by exposing nanotubes to sublimed fullerenes [1–5], virtually nothing is known about how the fullerenes enter the nanotubes when forming the nano-peapods.

A statistical mechanics approach, which considers only the initial and final states, describes only the equilibrium state after an infinite time [10]. It can say nothing about the likelihood of fullerene encapsulation in a finite time, as it ignores any activation barriers along the reaction path. Only trajectory calculations based on the complex potential energy surface of the system can provide detailed answers about the dynamics and intermediate steps involved in the formation of nano-peapods.

An important current controversy involves the questions, whether fullerenes enter through the open ends of perfect nanotubes or whether defects in the wall play an important role as entry channels. The extremely high filling ratio of up to 100% [5] appears hard to achieve even within a few days if the only entry channels are the two open ends of each tube. In such a case, the fullerene kinetics is limited and even a single impurity may block an entry channel. On the other hand, only a few openings in the tube walls have been observed in high-resolution transmission electron microscopy (HRTEM) images [11]. Another important question, which a statistical approach cannot answer, is whether the encapsulation process, be it through an open end or through a defect, occurs directly from the gas phase or involves a diffusive motion along the wall.

Here, we present a large-scale simulation for the entry of a C_{60} molecule into a $(10, 10)$ carbon nanotube via different scenarios, illustrated in Fig. 1. We consider the encapsulation through the open end of a free-standing nanotube [Fig. 1(a)] and through the open end of a nanotube bundle [Fig. 1(b)]. These scenarios are compared to the C_{60} entry through a defect, in our model a large opening in the nanotube wall [Fig. 1(c)] [12]. Formation of such large defects may occur, we believe, during the harsh purification process that is a necessary prerequisite for peapod formation [4]. By assuming that the C_{60} adsorbs on the wall prior to encapsulation, we take advantage of the enhanced probability of the fullerene to find an entry channel into a nanotube within the lower-dimensional phase space probed by the C_{60} diffusing along the wall, as compared to a fullerene in the gas phase. Our calculations elucidate not only which of these processes is most likely but also the optimum temperature window for the peapod formation.

We calculate the potential energy of the fullerene-nanotube system using an electronic Hamiltonian that was used successfully to describe the formation of multiwall nanotubes [13] and the dynamics of a "bucky-shuttle" device [7]. This approach describes accurately not only the covalent bonding within the graphitic substructures but also the modification of the fullerene-nanotube interaction due to the interwall interaction and possibly the presence of unsaturated bonds at defect sites or tube edges [14]. We find the use of an electronic Hamiltonian to be required in this system, as analytical bond-order potentials do not describe the rehybridization at defect sites and tube ends with sufficient precision. Once the quantum nature of the interatomic interactions has been taken into account, the trajectories of the heavy carbon atoms are described reliably in a classical manner.

In Fig. 1 we present schematic views of the encapsulation scenarios together with the calculated potential energy surfaces in the x-y plane that contains the tube axes, the center of the C_{60} molecule, and the defect. The tube structures underlying the potential energy surfaces have been globally optimized. They reflect the relaxation at the open end of the tube and the edges of a large defect in the tube wall, representing an extended vacancy formed during the harsh purification process [15].

When following an "optimum" trajectory starting outside the tube, a C_{60} molecule may first physisorb on the outer wall, thus gaining ≈0.07 eV. Our energy contour plots in Fig. 1 suggest that the fullerene diffuses virtually freely along the tube wall. Since the adsorption potential
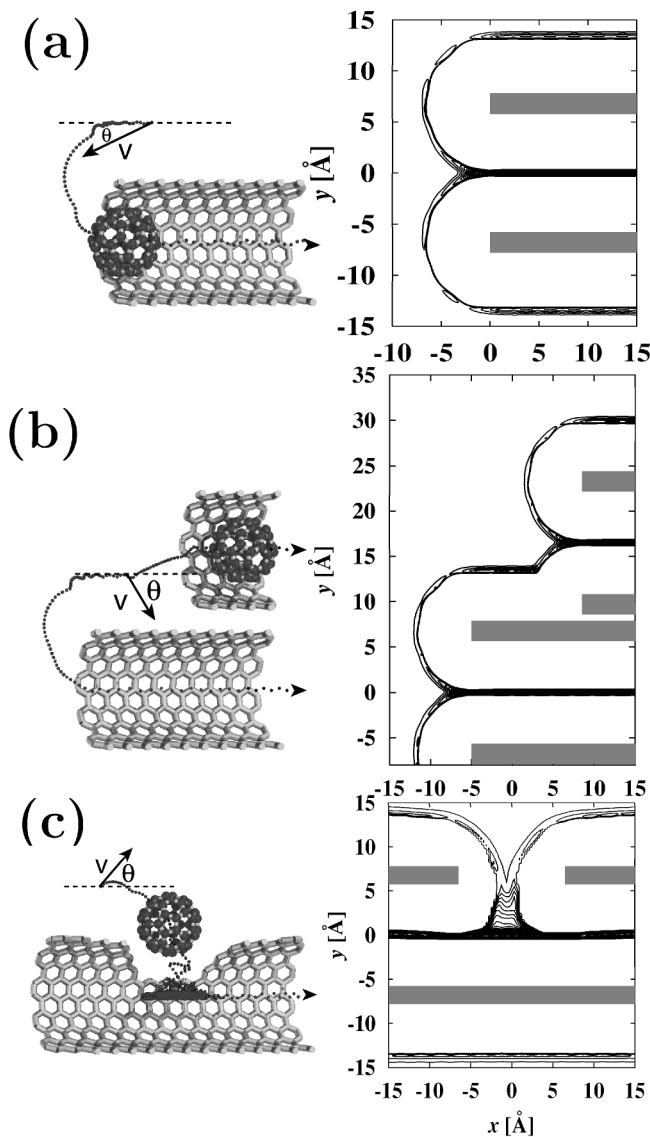
FIG. 1. Perspective views (left panels) and potential energy surfaces (right panels) for the encapsulation of a C_{60} molecule in a $(10, 10)$ nanotube under different scenarios. The dotted lines indicate possible C_{60} trajectories, characterized by the launch velocity v and launch angle θ with respect to the tube axis. The potential energy surfaces are shown in the x-y plane containing the center of the fullerene and the tube axis x. Adjacent energy contours are separated by 0.01 eV; the position of the tube walls is indicated by the solid gray areas. The scenarios involve C_{60} encapsulation through (a) the open end of an isolated $(10, 10)$ nanotube, (b) the open end of bundled $(10, 10)$ nanotubes, and (c) a large opening in the $(10, 10)$ nanotube wall, centered in the x-y plane.

is relatively shallow, the fullerene's angular velocity along the perimeter is limited by requiring the centrifugal force not to exceed a critical value for radial detachment. Consequently, the fullerene should follow a near-axial helical trajectory within a narrow 1D channel in the x-y plane during its diffusive motion along the tube surface. Because of the large inertia of the C_{60} molecule and the absence of corrugations along the potential energy surface, virtually

no rotations are excited as the fullerene slides along the tube wall. Upon entering the nanotube, the C_{60} gains an additional 0.36 eV [16].

The absence of activation barriers for all fullerene encapsulation scenarios depicted in Fig. 1 is surprising for two reasons. First, it suggests that the strong attraction to the undercoordinated atoms at the tube or defect edges does not trap the fullerene, but only modifies the entry channel without hindering the encapsulation [14]. Second, it leaves the origin of the observed optimum temperature of ≈ 400 °C for C_{60} encapsulation an open question.

The likelihood of C_{60} encapsulation depends on its initial conditions and the topology of the entire potential energy surface, as suggested by the sample trajectories in Fig. 1. In our molecular dynamics simulations, we initially placed the C_{60} molecule at equilibrium radial distance from the tube. We then calculated C_{60} trajectories in the x-y plane using time steps of 5×10^{-16} s, by varying the launch speed v from 0–300 m/s in 1 m/s increments and the launch angle θ with respect to the tube axis from $-90°$ to $+90°$ in 1° increments. The calculation of all 54 000 trajectories for each encapsulation pathway would not be computationally feasible without approximations. We described the fullerene-nanotube interaction by the potential energy surfaces presented in Fig. 1, thus implying that both the C_{60} and the nanotube are structurally rigid.

For each set of initial conditions, we found that the ultimate outcome of each trajectory regarding encapsulation is decided within less than 10^6 time steps. We also found that all physically interesting phenomena occur within a velocity range between 50–200 m/s, the lower bound marking the onset of C_{60} mobility along the tube. The upper end of this range corresponds to high temperatures, at which fragmentation and tube fusion are to be expected. Consequently, we will discuss the encapsulation under the specific scenarios within this velocity range.

The outcome of the encapsulation process through the end of an isolated nanotube, depicted in Fig. 1(a), is shown in Fig. 2. The scatter diagram of Fig. 2(a) condenses the information of all trajectories regarding encapsulation. A black mark denotes a trajectory with a launch velocity and angle that leads to encapsulation, such as that shown in Fig. 2(b). Similarly, a white field marks failed encapsulation, such as depicted in the trajectory of Fig. 2(c). Consequently, the fraction of the dark area is proportional to the probability of encapsulation. The scatter diagram, dominated by white color, suggests that encapsulation through the open end of an isolated nanotube should be very rare. The main reason is the relatively narrow and shallow channel in the potential energy surface of Fig. 1(a), which the fullerene must follow to reach the inside of the tube. At very low velocities, the fullerene gets trapped in one of the shallow potential energy wells outside the tube wall. At too high velocities, on the other hand, the C_{60} is incapable of following the tight "U turn" in the potential energy surface, as illustrated in Fig. 2(c).
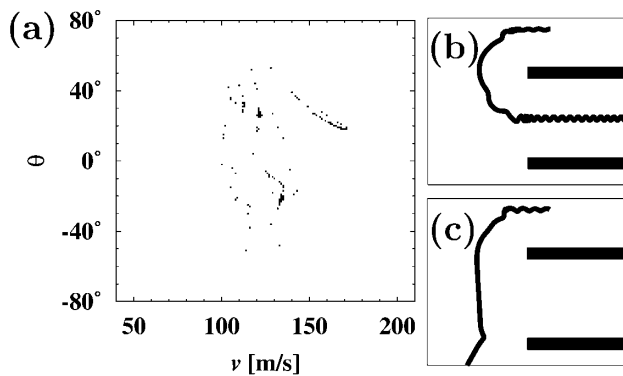
FIG. 2. (a) Scatter diagram showing the probable outcome of a C_{60} encapsulation through the open end of an isolated (10, 10) nanotube, as a function of the fullerene launch velocity v and launch angle θ. Only initial conditions leading to a successful encapsulation are marked in black in the scatter diagram. A sample successful encapsulation trajectory is depicted in (b), and an unsuccessful trajectory in (c).

In view of the low estimated probability of encapsulation through the end of an isolated tube, we considered next the analogous process at the end of a nanotube bundle, consisting of (10, 10) tubes with an interwall separation of 3.4 Å, depicted in Fig. 1(b). As suggested by the two successful trajectories in the left panel of Fig. 1(b), the more complex potential energy surface for this system increases the number of entry channels, thus enhancing the probability of encapsulation. The results of our trajectory calculations, summarized in the scatter diagram of Fig. 3(a), indeed show a somewhat higher encapsulation probability as compared to the single-tube scenario. In comparison to Fig. 2(a), we observe two solid dark regions for velocities beyond ≈150 m/s and $\theta \approx \pm 40°$. These regions correspond to trajectories that first follow the wall of one tube and continue inside the neighboring tube, as shown in Fig. 2(b). This new channel is relatively narrow due to the "S" shape of the tube-fullerene interaction potential well, shown in the right-hand panel of Fig. 1(b). As in the case of an isolated tube, trajectories involving a "U turn", depicted in Fig. 3(c), form an additional entry channel, responsible for the rare encapsulation events in the remaining region of the scatter diagram. We conclude that, even in the case of a bundle, the probability of encapsulation through the end is rather low.

The outcome of the encapsulation process through a large opening in the side wall of the (10, 10) nanotube, depicted in Fig. 1(c), is shown as a scatter diagram in Fig. 4(a). In comparison to Figs. 2(a) and 3(a), the dark area in the scatter diagram of Fig. 4(a) is substantially larger, yielding a 30-fold increase of the cross section for the C_{60} entry. In the following, we focus on the encapsulation through the large wall opening as the most likely process leading to peapod formation.

The scatter diagram of Fig. 4(a) shows a complex pattern consisting of large areas corresponding to the C_{60} entering the tube. Among these events, we have marked
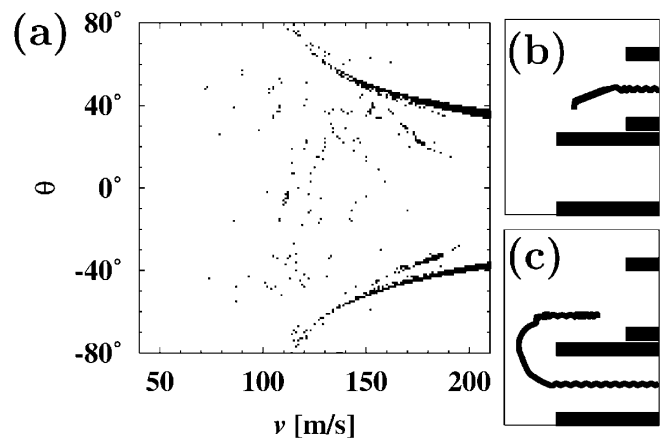

FIG. 3. Scatter diagram analogous to Fig. 2, but for bundled (10, 10) nanotubes. Sample trajectories describing successful encapsulation are depicted in (b) and (c).

those trajectories leading to a definitive encapsulation, as depicted in Fig. 4(b), in red. The "green" and "blue" trajectories, shown in Figs. 4(c) and 4(d), involve a temporary entry of the C_{60} molecule into the tube. In that case, after multiple scattering events, the fullerene may eventually escape in the backward ("green event") or the forward direction ("blue event"). Since such multiple scattering processes are chaotic, the blue and green events are homogeneously intermixed rather than separated into specific regions in Fig. 4(a).

To interpret the complex pattern in the scatter diagram of Fig. 4(a), we took a closer look at the individual trajectories. For launch velocities below 50 m/s, the C_{60} becomes trapped in one of the local minima and never reaches the
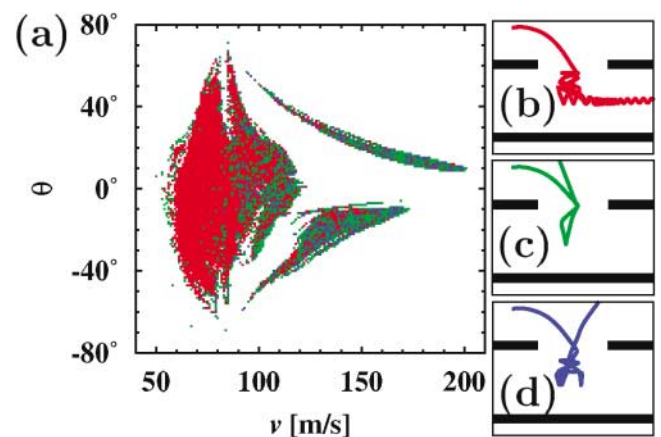

FIG. 4 (color). (a) Scatter diagram showing the probable outcome of a (10, 10) encapsulation through a large opening in the wall of a (10, 10) nanotube. Initial conditions that do not lead to encapsulation are marked in white. Those leading to encapsulation, with a sample trajectory shown in (b), are marked in red. Initial conditions and corresponding trajectories involving a temporary entry of the fullerene into the tube are shown in green if the final velocity has a negative x component (c) and in blue if the final velocity has a positive x component (d).

defect. The highest probability of a successful encapsulation with an axial launch ($\theta = 0°$) is achieved at velocities ranging from 50 m/s $\lesssim v \lesssim$ 120 m/s. Axial launches with velocities exceeding $\approx$120 m/s overshoot the hole. C_{60} encapsulation is still possible for fast launches, but requires large launch angles and involves one or several radial reflections off the wall, as shown schematically in Fig. 1(c). For a given nonzero launch angle, the largest launch velocity allowing the fullerene to enter the tube involves a straight trajectory with no radial reflections. This is the case for the trajectories depicted in Figs. 4(b)–4(d), for launch angles $\theta \approx 10°$ and $v \lesssim$ 200 m/s. At lower launch velocities, a radial reflection from the tube wall causes the fullerene to overshoot the hole. As the velocity is reduced further, the point of first radial reflection is shifted closer to the launch site, allowing the fullerene to successfully enter the nanotube again. At a constant launch angle such as $\theta = 40°$, we can distinguish up to seven alternating regions associated with "successful" and "unsuccessful" trajectories. Each of these contiguous regions in Fig. 4(a) can be characterized by the number of radial reflections between the launch site and the hole edge.

Maybe our most important result is the finding that, in the absence of inelastic scattering, the probability of successful encapsulation ("red" events) is largest in the velocity range between 80–120 m/s and almost independent of the launch angle θ. This suggests that not the launch direction but rather the kinetic energy of the C_{60} molecule decides the outcome. In view of the restricted motion of the C_{60} molecule along the tube surface, which reduces the number of degrees of freedom, we find that this velocity window translates into a kinetic temperature of the C_{60} close to 400 °C.

It is remarkable that the optimum temperature for peapod formation, as predicted by our calculation, falls into the observed temperature range from (350–450) °C [4]. Previous explanations of this optimum temperature window were based only on plausibility arguments suggesting a low C_{60} mobility at low temperatures and a closure of the wall defects or fullerene fusion [17] under annealing conditions. We believe that the quantitative agreement between theory and observation also provides indirect evidence that the microscopic encapsulation mechanism involves defects in the tube wall.

Our assumption that the microscopic degrees of freedom are decoupled from the macroscopic motion of the C_{60} molecule gained us 5 orders of magnitude in computing efficiency. Clearly, the possibility of energy transfer between the macroscopic and microscopic degrees of freedom introduces a damping mechanism. This new inelastic channel could convert some of the green and blue trajectories, depicted in Fig. 4, into successful encapsulation events, thus further increasing the cross section for C_{60} encapsulation.

In summary, we studied the microscopic formation mechanism of $(C_{60})_n@$ $(10, 10)$ peapods by considering the fullerene entry through an extended vacancy in the wall and the open end of isolated or bundled tubes. Our total energy calculations indicate that the encapsulation process does not involve activation barriers. Extensive molecular dynamics simulations, performed under the different scenarios as a function of the C_{60} launch velocity and direction, indicate that the most likely encapsulation occurs through a large opening in the tube wall, within a narrow range of launch velocities that agrees well with the experimentally observed temperature window. Increasing concentration of defects will improve the encapsulation efficiency up to the point where, due to a significant fraction of atoms missing or displaced, the tubes lose their structural integrity.

*Present address: Nanomix, Inc., 1295A 67th Street, Emeryville, California 94608.

[1] B. W. Smith, M. Monthioux, and D. E. Luzzi, Nature (London) **396**, 323 (1998).

[2] B. Burteaux *et al.*, Chem. Phys. Lett. **310**, 21 (1999).

[3] B. W. Smith, M. Monthioux, and D. E. Luzzi, Chem. Phys. Lett. **315**, 31 (1999).

[4] B. W. Smith and D. E. Luzzi, Chem. Phys. Lett. **321**, 169 (2000).

[5] K. Hirahara *et al.*, Phys. Rev. Lett. **85**, 5384 (2000).

[6] J. Sloan *et al.*, Chem. Phys. Lett. **316**, 191 (2000).

[7] Y.-K. Kwon, D. Tománek, and S. Iijima, Phys. Rev. Lett. **82**, 1470 (1999).

[8] Robert F. Service, Science **292**, 45 (2001).

[9] L. A. Girifalco, M. Hodak, and R. S. Lee, Phys. Rev. B **62**, 13104 (2000).

[10] M. Hodak and L. A. Girifalco, Phys. Rev. B **64**, 035407 (2001).

[11] M. Monthioux *et al.*, Carbon **39**, 1251 (2001).

[12] We propose that what has been interpreted as harmless "amorphous overcoating" of perfect single-wall nanotubes in HRTEM images may indeed represent defective nanotube segments with openings large enough to let a fullerene pass through.

[13] Y.-K. Kwon *et al.*, Phys. Rev. Lett. **79**, 2065 (1997).

[14] Because of their enhanced reactivity, unsaturated edges form a stronger bond with the fullerenes than edges saturated with hydrogen or other elements. It is conceivable that fullerenes could get trapped near vacancies that are smaller or comparable in size with the fullerene.

[15] We consider a defect formed by removing 76 atoms from the wall, with a diameter of $\approx$13.6 Å, just large enough to permit an unhindered entry of a C_{60} molecule.

[16] Susumu Okada, Susumu Saito, and Atsushi Oshiyama, Phys. Rev. Lett. **86**, 3835 (2001).

[17] S. Bandow *et al.*, Chem. Phys. Lett. **337**, 48 (2001).